Available online at www.sciencedirect.com
ScienceDirect
Ceramics International 35 (2009) 2171–2178
CERAMICS INTERNATIONAL
www.elsevier.com/locate/ceramint

Influence of microstructure and phase composition on the nanoindentation characterization of bioceramic materials based on hydroxyapatite

C.Y. Tang [a], P.S. Uskokovic [b], C.P. Tsui [a], Dj. Veljovic [b], R. Petrovic [b], Dj. Janackovic [b,*]

[a] *Department of Industrial and Systems Engineering, The Hong Kong Polytechnic University, Hung Hom, Kowloon, Hong Kong, PR China*
[b] *Faculty of Technology and Metallurgy, University of Belgrade, Karnegijeva 4, 11000 Belgrade, Serbia*

Received 12 September 2008; received in revised form 15 October 2008; accepted 27 November 2008
Available online 14 January 2009

Abstract

The aim of the study was to investigate the influence of microstructure and phase composition on the mechanical behaviour of hydroxyapatite (HAp) and biphasic HAp/β-tricalcium phosphate (β-TCP) bioceramic materials using nanoindentation. The formation of β-TCP phase in the HAp ceramic had the predominant influence on the nanomechanical properties of compact ceramics. For investigated microstructures there appear to be a slight decrease in the elastic modulus with increasing load and a higher decrease in hardness, which are in agreement with upper bounds of the results reported in literature. Maximal value of reduced modulus and hardness is yielded with pure HAp, and is measured to be 133.76 GPa for average grain size of 3 μm and 12.18 GPa for average grain size of 140 nm, respectively. The average modulus and hardness results for HAp/β-TCP ceramics with higher (101.61 GPa, 6.76 GPa) and lower grain size (115.72 GPa, 8.76 GPa) show sufficient mechanical properties in order to serve as hard tissue replacement material.

Keywords: B. Grain size; C. Mechanical properties; D. Apatite; Nanoindentation

1. Introduction

Calcium hydroxyapatite, $Ca_{10}(PO_4)_6(OH)_2$, has a wide range of biomedical applications because it is bioactive and biocompatible material and structurally similar to bone and tooth mineral [1]. Dense sintered form of calcium hydroxyapatite is clinically very important for bone reparation, tooth root replacement procedures, augmentation of alveolar ridges, pulp capping, maxillofacial reconstruction etc. [2,3].

Development of dense hydroxyapatite ceramics with superior mechanical properties is possible if the starting powder is stoichiometric with better powder properties such as crystallinity, agglomeration, and morphology [4]. Given their poor sinterability, HAp ceramics show insufficient mechanical properties, especially in wet environments as could be found in physiological conditions. During the past decade, major advances have been made in developing bioceramic microstructures, in order to obtain implant material for hard tissue replacement with better mechanical properties. A decrease in grain size from microscale to nanoscale in dense sintered materials is one of the main stream approaches to enhance the mechanical and biological properties of HAp-based bioceramic materials [5,6].

High sintering temperatures and long sintering duration required for consolidation of HAp powders often result in extreme grain coarsening and decomposition of HAp, resulting in degradation of its mechanical properties [7]. Nanostructured ceramics are usually processed by compacting nanopowders at high pressures and sintering at different times and temperatures and in various atmospheres [8]. Pressure assisted methods, such as hot pressing, hot isostatic pressing, sinter forging, etc, are also applied to obtain nanostructured ceramic materials. Hot pressing makes it possible to enhance densification kinetics and limit grain growth [9–12].

During sintering and hot pressing, the calcium deficient apatite turns into a mixture of HAp and β-TCP. A high amount of β-TCP is highly detrimental to the sintering and mechanical properties of HAP bioceramics [13]. In order to avoid degradation of the mechanical properties, the absence of the β-TCP in HAp bioceramic materials is advisable. On the other

* Corresponding author. Tel.: +381 11 3370489; fax: +381 11 3370387.
E-mail address: nht@tmf.bg.ac.yu (D. Janackovic).

0272-8842/$34.00
doi:10.1016/j.ceramint.2008.11.028

hand, the rate of degradation and bioactivity for calcium phosphate ceramics can be controlled by combining HAp and β-TCP.

Because of the brittle and fragile properties of bioceramics, such as HAp and TCP, applied loads of 10-500 grams such as for Vickers indentation are comparatively too large to measure their mechanical properties. In particular, surface mechanical properties such as hardness could be grain-size dependent. In contact mechanics, hard materials like ceramics are stressed in very small areas. From this point of view, nanoindentation is proven to be powerful method for elucidating mechanical properties at nanoscale level, comparable to the mean grain size of ceramic materials. Besides in a number of materials such as thin films and hard coatings, fine grained ceramics, polymers and composites [14–17], characterization of mechanical properties in fine spatial resolutions is recently applied to a range of biomaterials such as ultra-high-molecular-weight polyethylene, sintered bioceramic powders and functionally graded bioactive composites [18–21].

The aim of this work was the processing of dense nanostructured HAp bioceramic materials, obtained by sintering and hot pressing of nanosized HAp powder, in order to investigate effects of grain size and presence of β-TCP on nanomechanical properties of these materials.

2. Experimental

Two different modified chemical precipitation syntheses were used to obtain calcium deficient and stoichiometric nanosized HAp powders. Calcium hydroxyapatite, HAp1, was obtained by the reaction of H_3PO_4 and CaO, obtained by calcination of $CaCO_3$ at 1100 °C. Calcium oxide was suspended in distilled water and phosphoric acid was added at the rate of 1 cm^3/min, until the end point was reached (pH 7). The reaction took place in a 1 dm^3 reaction vessel, at 25 ± 1 °C, equipped with mechanical stirrer, condenser, electrical heater with contact thermometer, combined pH electrode, peristaltic pump for phosphoric acid, and a tube for N_2 addition [22]. After titration and aging (during 24 h), HAp suspension was filtrated in a Buchner funnel, washed by distilled water, dried at 105 °C and grained in a mortar.

Powder HAp2 was obtained at 94 ± 1 °C. A calculated amount of diluted 85% (1:1) phosphoric acid was added dropwise to the calcium hydroxide suspension. When all the necessary quantity of phosphoric acid was introduced pH reached the value 7.4–7.6. The obtained suspension was heated to 94 ± 1 °C for 30 min and stirred for another 30 min. After sedimentation, the upper clear solution layer was detached. The suspension was then spray-dried at 105 °C into granulated powder [23–25].

The synthesized HAp powders were isostatically pressed at 400 MPa, for 1 min, resulting into uniform green compacts, which were sintered at 1200 °C in air atmosphere for 2 h, in order to obtain uniform dense microstructure. The initial heating rate was 20 °C/min. In the following of experiment, isostatically pressed green compacts were hot pressed at 20 MPa in argon atmosphere, at 1000 °C for 1 h, in order to obtain uniform dense microstructure with significantly minor grain size then compact sintered at 1200 °C.

Powder morphology and particle size were evaluated using a transmission electron microscope (Philips EM400). The morphology of the green compacts was determined using scanning electron microscope (Jeol T-20). The specific surface area measurement was done using a BET surface area analysis. The morphology of the sintered and hot pressed compacts was examined with a scanning electron microscope (Jeol JSM 5800 and Jeol JSM-6460LV). The average grain size of the samples was determined by measuring grains from the fractured and polished/etched surfaces of the materials, and evaluated by image analysis of SEM micrographs, using software for image analysis, Image Pro Plus Program, version 4.0 for Windows. More than 100 HAp grains were counted to obtain an average value. FTIR analyses of the HAp powders and the sintered and hot pressed compacts were performed using an MB Bomen 100 Hartmann and Braun spectrometer in the wavenumber range from 400 to 4000 cm^{-1}. The samples were prepared by the KBr method at a sample ratio KBr = 1:150. X-ray diffraction analyses of HAp powders, sintered and hot pressed compacts were performed using the Philips PW1710 diffractometer with Cu Kα radiation and a graphite monochromator, with the angle 2θ ranging from 20° to 50° and the step scan of 0.02°. HAp compacts density was measured using Archimedes' method.

Nanoindentation experiments were carried out using a Triboscope Nanomechanical Testing System (Hysitron, Minneapolis, MN) equipped with a Berkovich indenter and *in situ* imaging mode. The frequently used method proposed by Oliver and Pharr [26], involves the extrapolation of a tangent to the top of the unloading curve to determine the depth (a combination of elastic and plastic deformation) over which the indenter is in contact with the specimen at the maximum load, P_{max} The slope of the unloading curve also provides a measure of the contact stiffness, which can be used with the contact area to determine the elastic modulus. The modulus obtained, sometimes referred to as the reduced modulus, E_r, which is related with material properties of indented specimen and indenter. If the stiffness of indenter is much greater than that of specimen, as is here, this relationship is given by: $E_r = E/(1 - \upsilon^2)$, where E is Young's modulus and υ is the Poisson's ratio of indented specimen. Nanoindentation tests were performed at two indentation loads, 1 and 2 mN. The indenter tip radius was estimated to be about 150 nm.

3. Results and discussion

The TEM images of the starting HAp1 and HAp2 nanopowders showed powders consisted of nanosized rod-shaped particles having 50–100 nm in size (Figs. 1 and 2). The SEM micrographs of the green compacts isostatically pressed at 400 MPa are shown in Figs. 3 and 4. The green compacts were dense and uniform, as the result of applied high isostatic pressure and the presence of soft aggregates in the starting HAp powders. The green compacts density of the HAp1 and HAp2 powders, were 1.76 g/cm^3 and 1.89 g/cm^3, or 56% and 59% of the theoretical density, respectively.

Fig. 1. TEM photograph of the HAp1 powder.

The Ca/P ratio of the HAp1 powder, as determined by ICP analyses, was 1.62 ± 0.01. This ratio shows that calcium deficient hydroxyapatite was obtained. The Ca/P ratio of the HAp2 powder was stoichiometric, 1.67 ± 0.01. The specific surface areas of HAp1 and HAp2 powder, determined by BET method, were $72 \pm 1\ m^2/g$ and $59 \pm 5\ m^2/g$, respectively.

The XRD patterns of the HAp powders showed a very low crystallinity (Fig. 5). The only peaks recognized were those corresponding to the calcium hydroxyapatite phase. All the peaks perfectly matched the JCPDS pattern 9-432 for HAp.

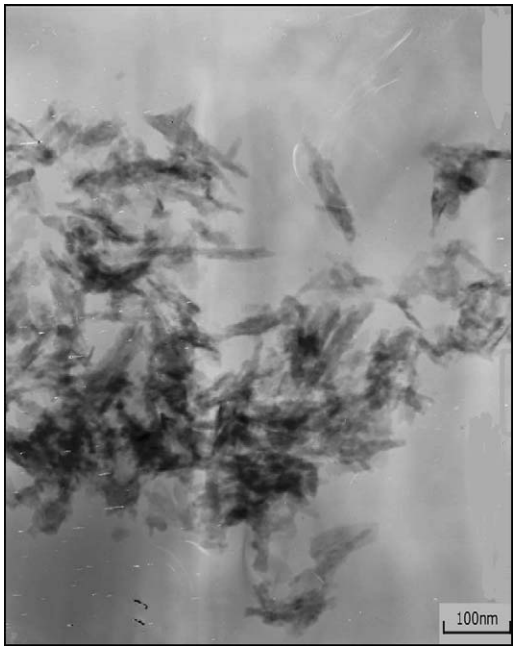

Fig. 2. TEM photograph of the HAp2 powder.

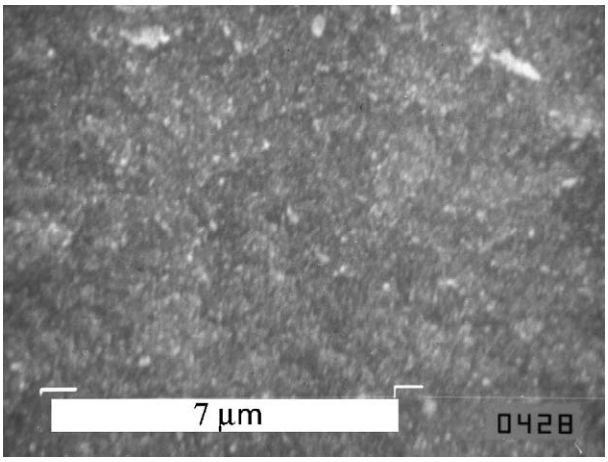

Fig. 3. SEM micrograph of a green compact of HAp1 powder pressed at 400 MPa.

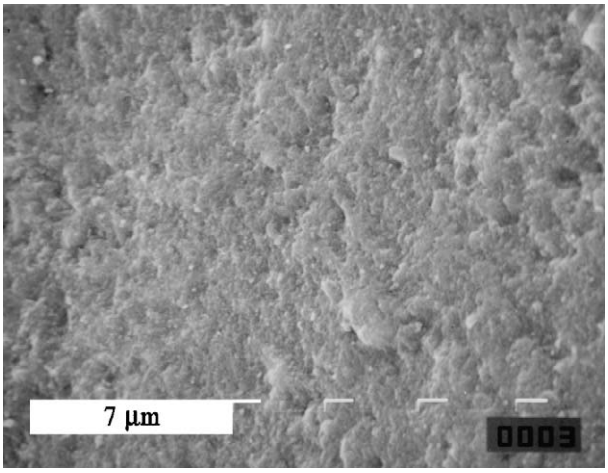

Fig. 4. SEM micrograph of a green compact of HAp2 powder pressed at 400 MPa.

The Fourier transform infra-red (FTIR) analysis of the HAp powders (Fig. 6) revealed the characteristic bands corresponding to calcium hydroxyapatite: the phosphate group bands at 462, 553, 595, 958, and 1024–1115 cm^{-1}, the OH^- group band at 3584 and 636 cm^{-1} and the HPO_4^{2-} band at 873 cm^{-1} [27].

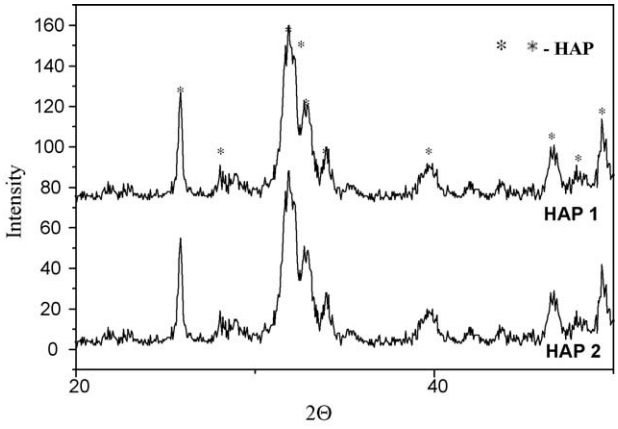

Fig. 5. XRD patterns of HAp1 and HAp2 powders.

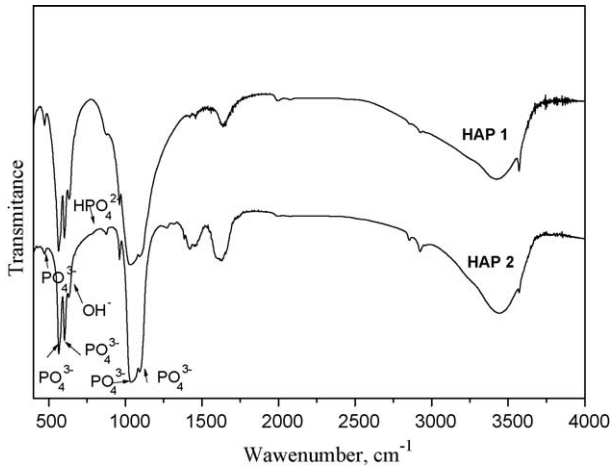

Fig. 6. FTIR spectra of HAp1and HAp2 powders.

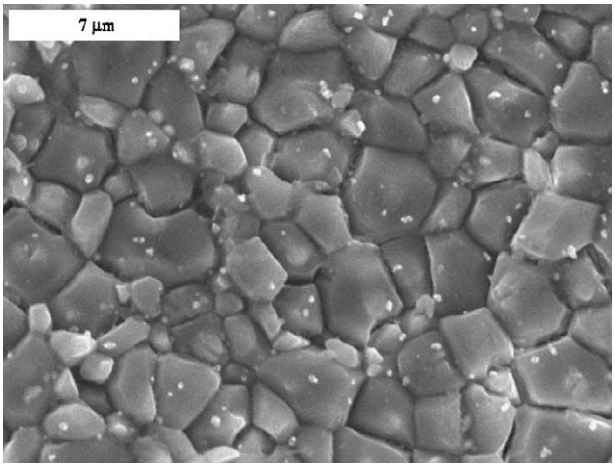

Fig. 7. SEM micrograph of a HAp1 sample sintered at 1200 °C for 2 h.

In order to investigate the effect of grain size and presence of β-TCP on nanoindentation test of bioceramics materials based on HAp, dense hydroxyapatite form were obtained by sintering and hot pressing of green compacts. The SEM micrographs of the compacts HAp1 and HAp2, sintered at 1200 °C for 2 h are shown at Figs. 7 and 8, respectively. Both of these microstructures were nonporous with around 3 μm mean grain size and slightly uniform grain sized distribution of powder HAp1.

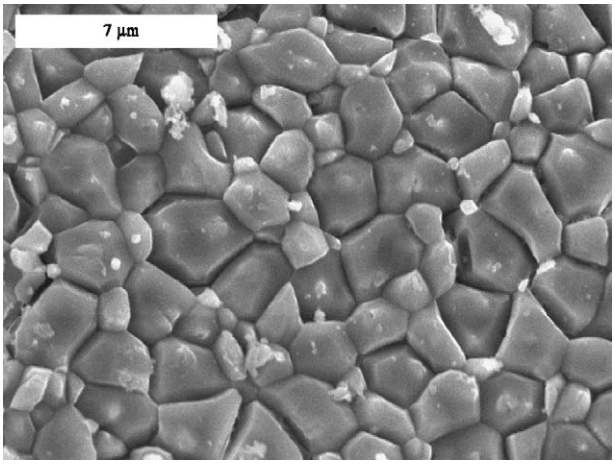

Fig. 8. SEM micrograph of a HAp2 sample sintered at 1200 °C for 2 h.

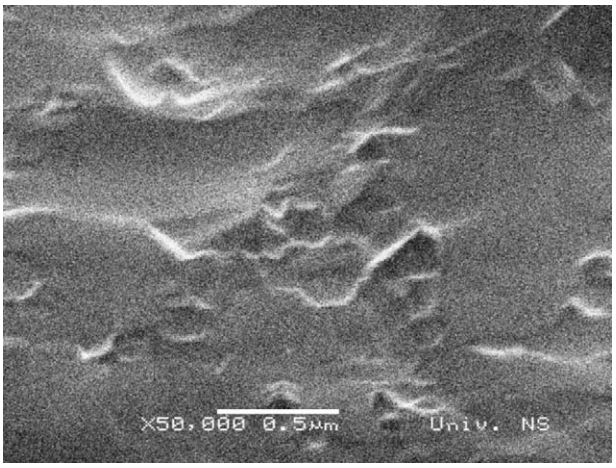

Fig. 9. SEM micrograph of a HAp1 sample hot pressed at 1000 °C for 1 h.

In the second part of the experiments, green compacts were hot pressed at 1000 °C for 1 h, resulting in full dense HAp compacts with certainly smaller grain size. The SEM micrographs of HAp1 and HAp2 compacts are shown in Figs. 9 and 10, respectively. Both of these microstructures were dense and translucent, with mean grain sizes of 170 nm and 140 nm, and densities of 3.10 g/cm^3 and 3.06 g/cm^3, respectively.

The FTIR analysis of the HAp1 and HAp2 samples sintered at 1200 °C for 2 h and hot pressed for 1 h at 1000 °C (Fig. 11) showed the characteristic bands corresponding to calcium hydroxyapatite. The XRD patterns of HAp1 samples sintered at 1200 °C for 2 h and hot pressed at 1000 °C for 1 h, in Fig. 12, show that sintered material is biphasic mixture of HAp and β-TCP, where the dominant crystalline phase of the sintered compacts is calcium hydroxyapatite. The XRD pattern of HAp2 samples sintered at 1200 °C for 2 h and hot pressed at 1000 °C for 1 h, in Fig. 12, shows peaks suggesting that HAp was the prevailing crystalline phase in the bioceramic materials obtained.

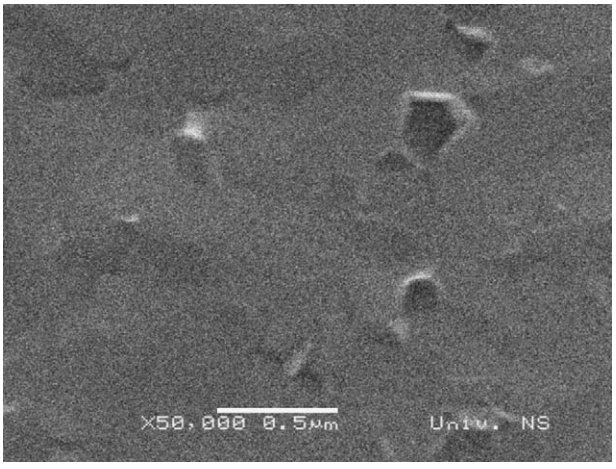

Fig. 10. SEM micrograph of a HAp2 sample hot pressed at 1000 °C for 1 h.

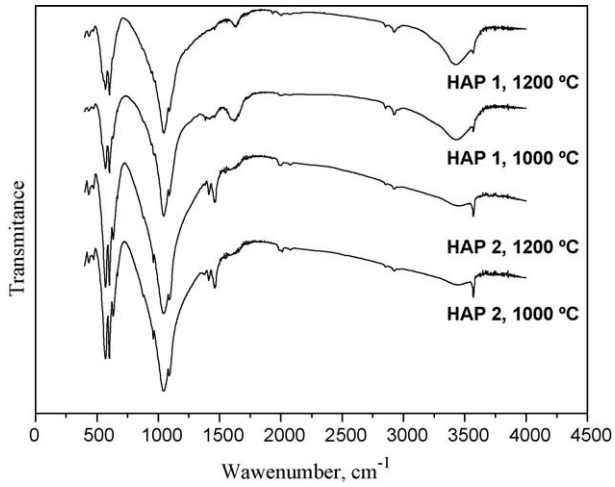

Fig. 11. FTIR spectra of HAp1 samples sintered for 2 h at 1200 °C and hot pressed for 1 h at 1000 °C, and HAp2 samples sintered for 2 h at 1200 °C and hot pressed for 1 h at 1000 °C.

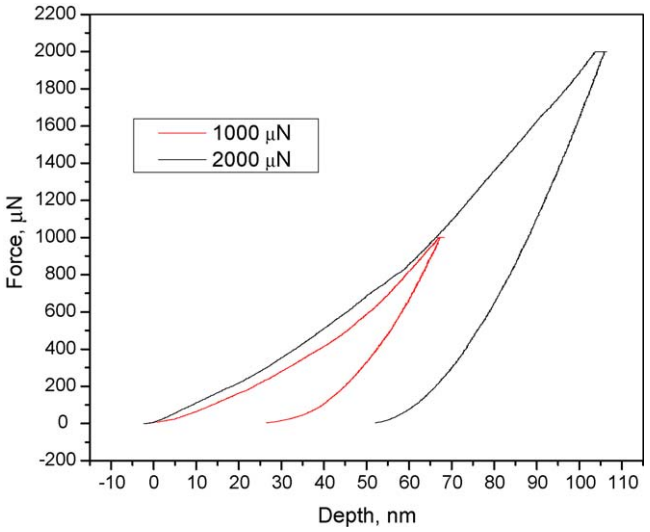

Fig. 13. Typical force–depth curves for sample S3 under both indentation loads.

The nanoindentation tests for dense compact materials with an applied load of 1 mN were conducted under the loading and unloading rate of 50 μN/s. In order to keep the total indentation rime of 60 s, for an applied load of 2 mN, the loading and unloading rate was set to be 100 μN/s with hold time of 20 s. The hold time step of 20 s at the both peak loads is used to minimize the creep effect, which could influence the shape of the unload curve and as a result might affect the calculated values of the Young's modulus and hardness. For the sake of brevity, the specimens of HAp2 and HAp1 with small grain size were denoted as S1 and S2 and specimens of HAp2 and HAp1 with larger grain size were denoted as S3 and S4, respectively.

Fig. 13 shows a typical force–depth curve obtained in the nanoindentation tests. The curves are characterized by a substantial continuity, i.e. without any large pop in or pop out, both in loading and unloading.

Images of the indents were captured using the same indenter in the scanning probe microscope (SPM) mode (Fig. 14), which confirms the absence of any cracks and fractures around the indent and clearly reveals material piled up at the edges of the indent. Flow of the material along the edges of indentation impressions is clearly presented in the 3D view of deformed surface (inset of Fig. 14), which is substantiated by a line profile across selected indent. Similar pile-ups around the indent were observed in hydroxyapatite single crystals, suggesting that nanoscale plasticity is a common phenomenon in calcium phosphate ceramics [28,29]. Hardness and modulus calculated according to the Oliver and Pharr model could be affected by pile-up especially when the ratio of contact depth to maximum displacement recorded during the test is higher than 0.7 [30]. However, this ratio in our tests was always below 0.7, which suggests that the calculated values of hardness and reduced

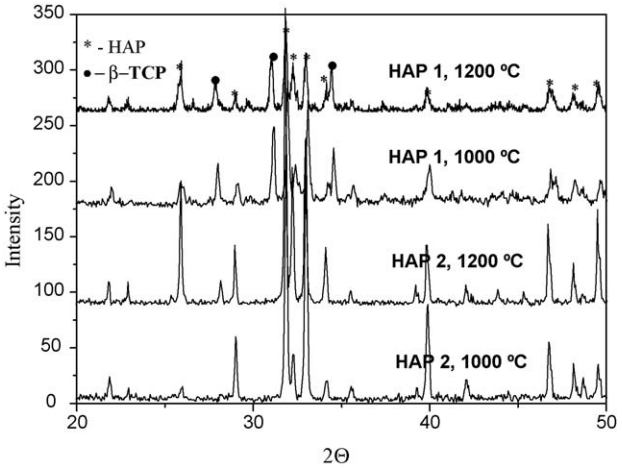

Fig. 12. XRD patterns of HAp1 samples sintered for 2 h at 1200 °C and hot pressed for 1 h at 1000 °C, and HAp2 samples sintered for 2 h at 1200 °C and hot pressed for 1 h at 1000 °C.

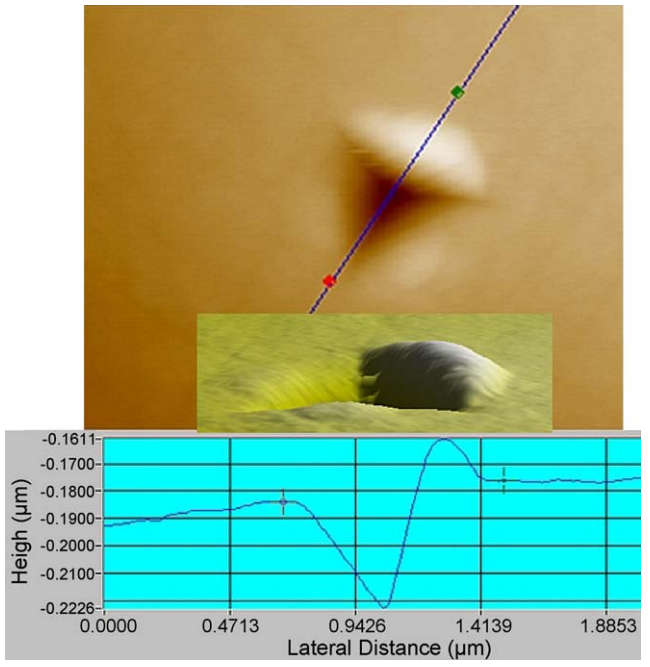

Fig. 14. SPM image with surface trace of S1 sample, indent force 2000 μN, scan size is 2 μm; region roughness is about 23 nm.

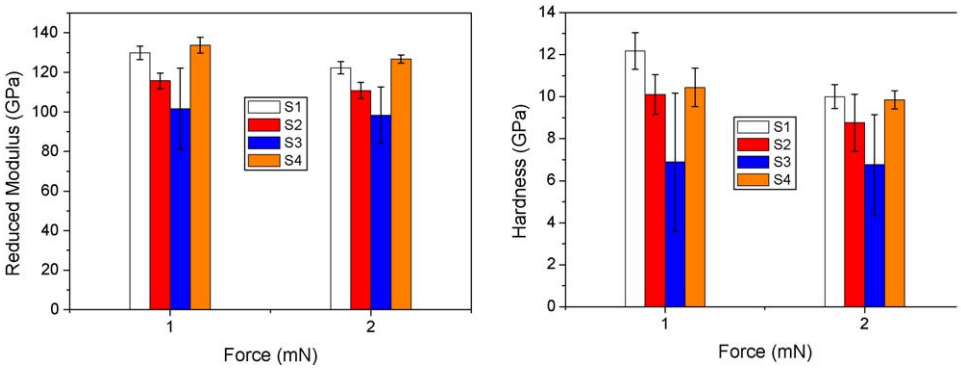

Fig. 15. Reduced modulus and hardness for samples tested in nanoindentation.

modulus should not be significantly affected by the presence of pile-up.

Hardness and reduced modulus of the processed ceramics with various microstructures and phase compositions are shown in Fig. 15 as a function of peak load. For both grain size and indentation forces, reduced modulus and hardness values are higher for pure HAp ceramic (S1, S4) than for HAp/β-TCP (S2, S3), confirming the prevailing effect of the β-TCP phase content on the nanomechanical properties. Furthermore, the higher standard deviation from the HAp/β-TCP samples tests also reflected the inhomogeneous properties of local surface areas due to formation of the second phase. Another possible explanation related to porosities is eliminated from this study because of the dense microstructure of all the tested samples.

The results in Fig. 15 indicate that there appears to be a slight decrease in the elastic modulus with increased load and a higher decrease in hardness, thus indicating the indentation size effect (ISE). Among several possible explanations for the load-dependent material behaviour, He et al. [31] discussed that for HAp nanoindentation testing, at higher contact loads a larger plastic core will be generated and more damage, in the form of cracks and fracture may be introduced into the plastic-deformed core. Bearing in mind applied indentation forces of other studies for HAp and the absence of damage in the vicinity of indents (Fig. 14), this was not likely to be explanation for ISE in this study. More feasible explanation could be that the polishing procedure may have introduced a surface densified layer which contained some residual stresses. The higher standard deviation from the lower-load tests also reflected the inhomogeneous properties of local surface areas, which may point out that the modulus and hardness from higher load of 2 mN could be more accurate reflection of the properties of bulk materials with the confidence that the crack and damage will not occur. For an indication, the difference between hardness for peak loads of 1 and 2 mN for S1 sample was 17.9%. Differences in average hardness for other samples, namely, S2, S3, S4, were 13.4%, 1.9% and 5.7%, respectively. Ceramics with smaller grain size show higher load dependence hardness behaviour. Similar trend for reduced modulus in dependence of applied load was observed. Differences between average reduced modulus for peak loads of 1 and 2 mN were modest and falling between 3.2% and 5.9% for S3 and S1, respectively. Nanoindentation characterization of liquid-phase-sintered SiC ceramic [32] indicate that the ISE is related to the mean grain size in that the hardness variation with the indentation depth, i.e. ISE, becomes an experimentally evident phenomenon only when the indentation depth remains confined to a dimension which is smaller than the mean grain size of the material. In the current investigation for all tested configurations, indentation depth does not exceed 110 nm and the lowest mean grain size is measured to be 140 nm.

By comparing the nanomechanical behaviour of samples with various grain sizes we could draw some conclusions which could benefit in the choice of appropriate processing conditions and the evaluation of pros and cons for the presence of softer but more biocompatible β-TCP phase in order to match desired mechanical properties of the implant material. For pure HAp, the decrease of grain size leads to the increase of hardness and decrease of modulus, larger for 1 mN and modest for 2 mN. By analyzing the nanoindentation results of HAp/β-TCP samples, we can conclude that the decrease of grain size yields the increase of both hardness and modulus. For both phase compositions tested, in correspondence of each peak load, the hardness of the materials was higher when the grain size was smaller. The increase of the hardness with the reduction of the mean grain size is usually described according to the Hall–Petch relation [33] to which these ceramics seem to conform. The fact that the material with the finer microstructure is stiffer than the same material with a coarser microstructure, as the case for HAp/β-TCP, was not an expected result. In fact, in small-grained materials the grain boundary phase, which is present with a high volumetric fraction with respect to a coarse-grained material, usually depresses the value of elastic modulus. However, Guicciardi et al. [34] reported that Y-TZP fine grains lead to a microstructural arrangement more compact and defect-free than coarser grains. Effects of the grain size on the mechanical properties were investigated mainly for nanocrystalline metals and a few ceramics based on models considering dislocations pile-up or composite approach. In these studies, there is a general agreement that the elastic modulus decreases with decreasing grain size, however without explanation of changes in the elastic modulus at the lower grain size range of the nanoscale regime [35]. Based upon experiences with aluminium oxide ceramics in conventional testing, Metsger et al. [36] concluded that it is unlikely that variances in grain sizes of HAp will affect Young's modulus

measured by conventional methods, and additionally pointed out that for nanomechanical characterization of materials with grain size in the nanometre regime, more experimental findings for various material configurations are needed.

The range of modulus and hardness values for both tested ceramic compositions and microstructural configurations is in good agreement with upper bounds of the results previously reported in literature [37–39], thus confirming the surface mechanical properties of HAp and HAp/β-TCP to be plausible as implant material for hard tissue replacement. Maximal value of reduced modulus and hardness was yielded with pure HAp, and was measured to be 133.76 GPa for average grain size of 3 μm and 12.18 GPa for average grain size of 140 nm, respectively. Viswanath et al. [28] reported that the average hardness and elastic modulus values of β-TCP single crystals obtained by nanoindentation are 7.68 GPa and 120.69 GPa, respectively, which are about 400% and 100% higher than the values of polycrystalline β-TCP sintered at 1200 °C as reported by Wang et al. [40]. The large differences between single crystal and polycrystalline material could be attributed to the defect-free nature of the miniature single crystals. In present work, the obtained average modulus and hardness results for HAp/β-TCP ceramics with larger and smaller grain size of (101.61, 6.76) GPa and (115.72, 8.76) GPa support the processing procedure, which could lead to dense compact ceramic with phase stability and sufficient mechanical properties and biocompatibility in order to serve as hard tissue replacement material.

4. Conclusions

The hardness and reduced modulus of processed HAp and HAp/β-TCP dense ceramic compacts have been evaluated using the nanoindentation technique. By analyzing nanoindentation results, it can be seen that the formation of β-TCP phase in the HAp ceramic had the predominant influence on the nanomechanical properties of compact ceramics. For all the microstructural configurations there appear to be a slight decrease in the elastic modulus with increasing load and a higher decrease in hardness, thus indicating the ISE.

For pure HAp, the decrease of grain size leads to the increase of hardness and decrease of modulus, larger for 1 mN and modest for 2 mN. By analysing the nanoindentation results of HAp/β-TCP samples it may be concluded that the decrease of grain size yields the increase of both hardness and modulus, which could be a consequence of a better microstructural arrangement. For both of the ceramic configurations tested, in correspondence of each peak load, the hardness of the materials was higher; the smaller was the grain size. The increase of the hardness with the reduction of the mean grain size is usually described according to the Hall–Petch relation to which these ceramics seem to conform.

The results of the current study are consistent with literature reports and suggest that the mechanical properties of HAp can be reasonably preserved by formation of TCP phase. The nanoindentation technique has a good potential for measuring the mechanical properties of brittle and fragile bioceramics, such as HAp and TCP ceramics. This study provides a contribution to developing stronger biomedical biphasic composites of HAp and β-TCP and for tailoring the biocompatibility demands without compromising the mechanical safety of the implant.

Acknowledgements

The authors would like to thank the substantial support from the Research Grants Council of Hong Kong (PolyU 5276/06E) and from the Ministry of Science and Technological Development of the Republic of Serbia through the project 142070.

References

[1] L.L. Hench, Bioceramics: from concept to clinic, J. Am. Ceram. Soc. 74 (1991) 1487–1510.
[2] R.Z. Legeros, J.P. Legeros, Dense hidroxyapatite, in: L.L. Hench, J. Wilson (Eds.), An Introduction to Bioceramics, World Scientific, Singapore, 1993, pp. 139–180.
[3] J.E. Barralet, G.J.P. Fleming, C. Campion, J.J. Harris, Formation of translucent hydroxyapatite ceramics by sintering in carbon dioxide atmospheres, J. Mater. Sci.: Mater. Med. 38 (2003) 3979–3993.
[4] N. Thangamania, K. Chinnakalib, F.D. Gnanama, The effect of powder processing on densification, microstructure and mechanical properties of hydroxyapatite, Ceram. Int. 28 (2002) 355–362.
[5] A. Banerjee, A. Bandyopadhyay, S. Bose, Hydroxyapatite nanopowders: synthesis, densification and cell–materials interaction, Mater. Sci. Eng. C 27 (2007) 729–735.
[6] W.D. Kingery, H.K. Bowen, D.R. Uhlman, Introduction to Ceramics, John Wiley and Sons, New York, 1976, p. 808.
[7] Y.W. Gua, K.A. Khora, P. Cheang, Bone-like apatite layer formation on hydroxyapatite prepared by spark plasma sintering (SPS), Biomaterials 25 (2004) 4127–4134.
[8] Dj. Veljovic, B. Jokic, I. Jankovic-Castvan, I. Smiciklas, R. Petrovic, Dj. Janackovic, Sintering behaviour of nanosized HAP powder, Key Eng. Mater. 330–332 (2007) 259–262.
[9] S. Raynaud, E. Champion, J.P. Lafon, D. Bernache-Assollant, Calcium phosphate apatites with variable Ca/P atomic ratio. III. Mechanical properties and degradation in solution of hot pressed ceramics, Biomaterials 23 (2002) 1081–1089.
[10] M.J. Mayo, Nanocrystalline ceramics for structural applications: processing and properties, in: G.M. Chow, N.I. Noskova, Nanostructured (Eds.), Materials Science and Technology, NATO ASI Series, Kluwer Academic Publishers, Russia, 1997, pp. 361–385.
[11] J.R. Groza, Nanosintering, Nanostruct. Mater. 12 (1999) 987–992.
[12] Dj. Veljović, B. Jokić, R. Petrović, E. Palcevskis, A. Dindune, I.N. Mihailescu, Dj. Janaćković, Processing of dense nanostructured HAP ceramics by sintering and hot pressing, Ceram. Int., in press.
[13] S. Raynaud, E. Champion, D. Bernache-Assollant, Calcium phosphate apatites with variable Ca/P atomic ratio. II. Calcination and sintering, Biomaterials 23 (2002) 1073–1080.
[14] C. Klapperich, K. Komvopoulos, L. Pruitt, Nanomechanical properties of polymers determined from nanoindentation experiments, ASME J. Tribol. 123 (2001) 624–631.
[15] J. Gong, Z. Peng, H. Miao, Analysis of the nanoindentation load–displacement curves measured on high-purity fine-grained alumina, J. Eur. Ceram. Soc. 25 (2005) 649–654.
[16] J.M. Torralba, F. Velasco, C.E. Costa, I. Vergara, D. Caceres, Mechanical behaviour of the interphase between matrix and reinforcement of Al 2014 matrix composites reinforced with (Ni3Al)p, Composites A 33 (2002) 427–434.
[17] M. Campo, A. Urena, J. Rams, Effect of silica coatings on interfacial mechanical properties in aluminium–SiC composites characterized by nanoindentation, Scripta Mater. 52 (2005) 977–982.

[18] K. Park, S. Mishra, G. Lewis, J. Losby, Z. Fan, J.B. Park, Quasi-static and dynamic nanoindentation studies on highly cross-linked ultra-high-molecular-weight polyethylene, Biomaterials 25 (2004) 2427–2436.
[19] R.R. Kumar, M. Wang, Functionally graded bioactive coatings of hydroxyapatite/titanium oxide composite system, Mater. Lett. 55 (2002) 133–137.
[20] V. Nelea, C. Morosanu, M. Iliescu, I.N. Mihailescu, Microstructure and mechanical properties of hydroxyapatite thin films grown by RF magnetron sputtering, Surf. Coat. Technol. 173 (2003) 315–322.
[21] C.Y. Tang, C.P. Tsui, Dj. Janackovic, P.S. Uskokovic, Nanomechanical properties evaluation of bioactive glass coatings on titanium alloy substrate, J. Optoelectron. Adv. Mater. 8 (2006) 1194–1199.
[22] I. Smičiklas, A. Onjia, S. Raičević, Experimental design approach in the synthesis of hydroxyapatite by neutralization method, Sep. Purif. Technol. 44 (2005) 97–102.
[23] M. Jarcho, C.H. Bolen, M.B. Thomas, J. Bobick, J.F. Kay, R.H. Doremus, Hydroxyapatite synthesis and characterisation in dense polycrystalline form, J. Mater. Sci. 11 (1976) 2027–2037.
[24] A. Osaka, Y. Miura, K. Takeuchi, M. Asada, K. Takahashi, Calcium apatite prepared from calcium hydroxide and orthophosphoric acid, J. Mater. Sci. Mater. Med. 2 (1991) 51–55.
[25] E. Palcevskis, A. Dindune, L. Kuznecova, A. Lipe, Z. Kanepe, Granulated composite powders on basis of hydroxyapatite and plasma-processed zirconia and alumina nanopowders, Latvian J. Chem. 2 (2005) 128–138.
[26] W.C. Oliver, G.M. Pharr, An improved technique for determining hardness and elastic modulus using load and displacement sensing indentation experiments, J. Mater. Res. 7 (1992) 1564–1583.
[27] R.N. Panda, M.F. Hsieh, R.J. Chung, T.S. Chin, FTIR, XRD, SEM and solid state NMR investigations of carbonate-containing hydroxyapatite nano-particles synthesized by hydroxide-gel technique, J. Phys. Chem. Solids 64 (2003) 193–199.
[28] B. Viswanath, R. Raghavan, N.P. Gurao, U. Ramamurty, N. Ravishankar, Mechanical properties of tricalcium phosphate single crystals grown by molten salt synthesis, Acta Biomater. 4 (5) (2008) 1448–1454.
[29] B. Viswanath, R. Raghavan, U. Ramamurty, N. Ravishankar, Mechanical properties and anisotropy in hydroxyapatite single crystals, Scripta Mater. 57 (2007) 361–364.
[30] A. Bolshakov, G.M. Pharr, Influences of pileup on the measurement of mechanical properties by load and depth sensing indentation techniques, J. Mater. Res. 13 (1998) 1049–1058.
[31] L.H. He, O.C. Standard, T.T.Y. Huang, B.A. Latella, M.W. Swain, Mechanical behaviour of porous hydroxyapatite, Acta Biomater. 4 (3) (2008) 577–586.
[32] S. Guicciardi, D. Sciti, C. Melandri, A. Bellosi, Nanoindentation characterization of submicro- and nano-sized liquid-phase-sintered SiC ceramics, J. Am. Ceram. Soc. 87 (2004) 2101–2107.
[33] R.A. Masumura, P.M. Hazzledine, C.S. Pande, Yield stress of fine grained materials, Acta Mater. 46 (1998) 4527–4534.
[34] S. Guicciardi, T. Shimozono, G. Pezzotti, Nanoindentation characterization of sub-micrometric Y-TZP ceramics, Adv. Eng. Mater. 8 (2006) 994–997.
[35] R. Chaim, M. Hefetz, Effect of grain size on elastic modulus and hardness of nanocrystalline ZrO_2-3 wt% Y_2O_3 ceramic, J. Mater. Sci. 39 (2004) 3057–3061.
[36] D.S. Metsger, M.R. Rieger, D.W. Foreman, Mechanical properties of sintered hydroxyapatite and tricalcium phosphate ceramic, J. Mater. Sci. Mater. Med. 10 (1999) 9–17.
[37] R.R. Kumar, M. Wang, Modulus and hardness evaluations of sintered bioceramic powders and functionally graded bioactive composites by nanoindentation technique, Mater. Sci. Eng. A 338 (2002) 230–236.
[38] E. Ho, M. Marcolongo, Effect of coupling agents on the local mechanical properties of bioactive dental composites by the nano-indentation technique, Dent. Mater. 21 (2005) 656–664.
[39] P.S. Uskokovic, C.Y. Tang, C.P. Tsui, N. Ignjatovic, D.P. Uskokovic, Micromechanical properties of a hydroxyapatite/poly-l-lactide biocomposite using nanoindentation and modulus mapping, J. Eur. Ceram. Soc. 27 (2007) 1559–1564.
[40] C.X. Wang, X. Zhou, M. Wang, Influence of sintering temperatures on hardness and Young's modulus of tricalcium phosphate bioceramic by nanoindentation technique, Mater. Charact. 52 (2004) 301–307.